HHS Public Access

Author manuscript

J Neural Eng. Author manuscript; available in PMC 2018 December 01.

Published in final edited form as:

J Neural Eng. 2017 December ; 14(6): 066014. doi:10.1088/1741-2552/aa814d.

Mechanical fatigue resistance of an implantable branched lead system for a distributed set of longitudinal intrafascicular electrodes

A E Pena[1], **S S Kuntaegowdanahalli**[1], **J J Abbas**[2], **J Patrick**[3], **K W Horch**[1], and **R Jung**[1]

[1]Florida International University, Department of Biomedical Engineering, Miami, FL, USA

[2]Arizona State University, School of Biological & Health Systems Engineering, Tempe, AZ, USA

[3]Cochlear Ltd., Sydney, Australia

Abstract

Objective—A neural interface system has been developed that consists of an implantable stimulator/recorder can with a 15-electrode lead that trifurcates into three bundles of five individual wire longitudinal intrafascicular electrodes. This work evaluated the mechanical fatigue resistance of the branched lead and distributed electrode system under conditions designed to mimic anticipated strain profiles that would be observed after implantation in the human upper arm.

Approach—Custom test setups and procedures were developed to apply linear or angular strain at four critical stress riser points on the lead and electrode system. Each test was performed to evaluate fatigue under a high repetition/low amplitude paradigm designed to test the effects of arm movement on the leads during activities such as walking, or under a low repetition/high amplitude paradigm designed to test the effects of more strenuous upper arm activities. The tests were performed on representative samples of the implantable lead system for human use. The specimens were fabricated using procedures equivalent to those that will be used during production of human-use implants. Electrical and visual inspections of all test specimens were performed before and after the testing procedures to assess lead integrity.

Main Results—Measurements obtained before and after applying repetitive strain indicated that all test specimens retained electrical continuity and that electrical impedance remained well below pre-specified thresholds for detection of breakage. Visual inspection under a microscope at 10X magnification did not reveal any signs of damage to the wires or silicone sheathing at the stress riser points.

Significance—These results demonstrate that the branched lead of this implantable neural interface system has sufficient mechanical fatigue resistance to withstand strain profiles anticipated when the system is implanted in an arm. The novel test setups and paradigms may be useful in testing other lead systems.

Keywords

peripheral nerve interface; neuroprosthesis; intrafascicular electrode; mechanical fatigue testing; electrode lead; implant; amputee; prosthesis

1. Introduction

Peripheral nerve interfaces enable uni- or bi-directional flow of information between the peripheral nervous system and a computing machine [1]. This technology has the potential to restore function after spinal cord injury, peripheral nerve injury or limb loss [2], or for use in autonomic control [3]. In general, a peripheral nerve interface consists of electrodes that interface with the nervous system and are connected via an electrode lead system to a stimulator/recorder electronics unit. Several types of electrodes are utilized for peripheral nerve interfaces [4–13]. The lead consists of the wires connecting the electrode or electrode array to the stimulating/recording device. Often the wires are bundled and coiled in order to provide strain relief and the bundle is enclosed in an external sheath [14–18]. Many peripheral nerve interfaces use a single multi-conductor lead, e.g., the fully implantable vagal nerve stimulator or the percutaneous tibial nerve stimulator [3, 19–21]. These leads are similar to those used to connect central nervous system electrodes to an electronics unit placed in the periphery, such as in spinal cord [22] or deep brain stimulation systems [23].

For many clinical applications, approaches that target peripheral nervous system structures may have advantages over those that target central nervous system structures, such as a reduction in the risks associated with implantation [24] and providing access to simpler, better understood neural codes [25]. One of the potential drawbacks of targeting the nerves in the periphery is that they slide and stretch while performing routine activities [1, 26–29]. This movement presents challenges to the stability of the electrode-nerve interface and the mechanical fatigue resistance of the leads, especially in systems where the electronics are housed at a distance from the electrode-nerve interface. Mechanical fatigue that causes lead breakage or cracks in the insulation or protective sheath around the electrode lead wires could reduce system functionality, increase risk, and/or constitute device failure. Lead systems such as those used in functional neuromuscular stimulators [30–36], spinal cord stimulators [22], and cardiac pacemakers [37–39] have been tested extensively both in-vitro and in-vivo to characterize the likelihood of long term survival under similar conditions.

In this work, we investigated the mechanical fatigue resistance of a branched, multi-conductor electrode lead system designed to interface with peripheral nerves. The lead system was developed as part of a neural-enabled prosthetic hand system designed to elicit sensations in amputees by electrically stimulating peripheral nerve fibers based on information derived from sensors in the prosthetic hand. At the core of this system is a device that includes an external processor and interface unit connected to the sensors in the prosthetic hand and an internal implantable stimulator/recorder (ISR). The ISR has a radio-frequency transmitting coil, a can to house electronics, and a 15-electrode array lead that trifurcates into three bundles of five individual longitudinal intrafascicular electrodes (LIFEs). The external interface unit and the internal ISR communicate via a wireless, transcutaneous link. The lead structure enables implantation of LIFEs in fascicles of peripheral nerves at distributed sites, e.g., in multiple nerves in the upper arm of an amputee [5, 40, 41]. This study characterized the mechanical fatigue resistance of this distributed, LIFE-based, branched lead system to conditions that mimic anticipated strain profiles in the upper arm. We fabricated modular testbeds and developed procedures to evaluate the susceptibility of the lead to damage at specific stress riser points when exposed to repetitive

linear and angular strains. Multiple tests were performed on representative samples of the implantable lead and electrodes for human use.

2. Methods

2.1. Implantable stimulator/recorder with a branched lead system and LIFEs

The implantable stimulator/recorder with the electrode lead bundle and LIFEs is shown in Figure 1A. The ISR is designed to be implanted in the upper arm to interface with multiple discrete groups of neurons distributed across fascicles in the major nerves of the arm. The ISR, which is encased in silicone, has a radio frequency (RF) coil and a hermetically sealed titanium can that houses the electronics for the system and has feedthroughs for 15 electrode wires bundled as a single lead and a ground lead. The overall size of the can with RF coil (approx. 30 mm × 50 mm) is similar to that of standard cochlear implants [42]. The electrode lead wires are made from 23 μm diameter Pt-Ir wires with an insulation thickness of ~4 μm. As shown in the schematic in Figure 1B, the 15 electrode lead wires exit the ISR as a single primary bundle and are coiled and ensheathed in medical grade silicone. The diameter of the primary bundle (1.19 mm) is similar to that of the lead in standard cochlear implants. The primary bundle extends for 15 cm from the ISR then branches at the trifurcation junction (TFJ) into three secondary bundles each with 5 lead wires to enable implantation of up to 5 LIFEs at each of three anatomical sites. The wires in the secondary bundles are also coiled and ensheathed up to the secondary bundle exit point, which is where the coiled lead wires separate into uncoiled individual wires. In each of the individual wires the electrode active site (exposed region) is formed by removing the insulation for a length of approximately 1 mm. The distal ends of the individual wires are welded to 75 μm diameter tungsten needles. All specimens used in this study were fabricated using materials that are identical to, and procedures that are equivalent to, those that will be used during production of implants for human use.

2.2. Stress Riser Points

A transition in size and/or stiffness along the length of the electrode lead can result in a localized concentration of stress that could eventually result in material failure such as lead breakage or cracks in the protective sheathing. [43]. Some of the stress riser points are at locations of structural transition along the length of the lead, while others are points where individual wires are surgically anchored. Figure 2A shows a schematic of the intended location of implantable components in the upper arm; Figure 2B shows a schematic of the electrode wires implanted in a nerve fascicle. During the implantation procedure, each electrode wire from a single secondary bundle is threaded into a fascicle using the tungsten needle, with one or more electrode wires per fascicle within the same nerve. All wires from a bundle are implanted at approximately the same longitudinal distance between the bundle exit and the nerve entry point, but at different locations around the circumference to access multiple sections of the same fascicle as well as different fascicles. Once all electrode wires from a secondary bundle are implanted at a given site, the longitudinal position of the active area for each electrode is adjusted so that it is within the fascicle. Subsequently, the distal portion of the wire is cut to remove the tungsten needles. The bundle exit point and the remaining portion of the wires left outside the nerve are sutured to the epineurium as shown

in Figure 2B. Our plan for surgical deployment is to use 9–0 nylon sutures (ETHILON Black 2813G, Ethicon), and therefore this material was used in the tests described below.

In the ISR lead system (Figure 1B, Figure 2), five prominent transition points are of concern: 1) the point where the single primary bundle of fifteen electrode wires ensheathed in silicone exits the distal end of the ISR can through a cone-like silicone tail; 2) the points where the secondary bundles exit the TFJ, which is a silicone structure that is stiffer than the bundle of electrodes; 3) the points where the individual electrode wires exit the secondary bundles; 4) the suture point where the secondary bundle is sutured to the nerve; and 5) the points where the individual wires are sutured in place after exiting the nerve.

2.3. Test Setups and Procedures

Fatigue testing of the stress riser points in the system required a series of setups capable of applying repetitive linear or angular strains to the test specimens. Each test setup was designed and built using off-the-shelf aluminum structural components and several custom-designed 3D printed parts. These custom parts were designed and fabricated in-house and a modular design approach was used. Aluminum parts were used in the primary load-bearing structures; 3D-printed parts, made of standard polylactic acid (PLA) plastic, were used for structures not exposed to substantial loads. The modular design allowed fine-tuning of the sample attachment structures and test parameters such as the direction and amplitude of the strain applied. The test setups were generally comprised of a motor sub-assembly to generate repetitive rotational motion, and consisted of a speed-controlled brushless DC motor (Anaheim Automation BLY17MDA) mounted on a 3D-printed base. A 3D-printed flywheel coupled to the motor allowed for multiple strain amplitude levels to be selected, using different linkage points along its radius. A linear or angular motion sub-assembly converted the rotational movement of the motor into linear or angular actuation. Specialized sample holders were designed to hold the test specimens and to apply strain at the stress riser point being tested. A linear strain testbed was used to test the junction where the primary bundle exits from the ISR can, the junction where the individual wires exit the secondary bundle, and the nerve suture points. An angular strain testbed was used to test the junction where the primary bundle exits from the ISR can and the trifurcation branching junction (Figures Figure 1B, Figure 4, Figure 5)

2.3.1. ISR Bundle Exit Linear and Angular Strain Tests—Each specimen used in these tests consisted of an ISR can, a single primary bundle with 15 coiled silicone ensheathed wires (CS1, L = 15cm), and the ground electrode lead (Figure 3A). At the proximal end of the specimen (i.e., the end with the ISR can), the 15 wires and the ground electrode were shorted to form a single electrical contact. At the distal end of the specimen, the 15 wires were attached to distinct contacts on a custom-designed printed circuit board (PCB) for electrical continuity monitoring.

In the ISR bundle exit linear strain test setup (Figure 4A), the proximal end of the specimen (ISR can) was clamped in one of three different orientations while the bundle's distal end was attached to a piston mechanism about 10 cm from the PCB. The piston mechanism used a brushless motor with an integrated speed controller coupled to a linear motion assembly to

apply longitudinal cyclic strain to the lead. The chosen orientations of the primary bundle position with respect to the ISR (Figure 4B) consisted of 1) 90° twist about the Y-axis and 90° bend about the Z-axis; 2) No bend; and 3) 90° bend around the Z-axis. These amplitudes and orientations were designed to represent worst-case scenarios in which the ISR lead exit point might experience very high strain in different directions.

The ISR bundle exit angular strain test setup (Figure 5A) consisted of a swinging fixture coupled to an oscillatory mechanism designed to apply repetitive angular strain to the ISR bundle exit point. The swinging fixture consisted of an ISR-shaped enclosure designed to hold the ISR can at two different orientations (0° and 90° about the Y-axis) in order to produce the desired bending angle (Figure 5B). The point at which the primary bundle exited the ISR can was placed at the center of oscillation, while the distal end of the bundle was fixed with a clamp, without applying any tension at the resting (0°) position. However, since the distal end of the bundle was clamped, the bundle was subjected to both angular and linear strain simultaneously at the peak of each bending cycle.

2.3.2. Trifurcation Junction Angular Test—Each specimen used in this test consisted of the trifurcation junction (TFJ) assembly (a single primary bundle with 15 coiled silicone ensheathed 15 cm long wires that trifurcated into three secondary bundles of five coiled silicone ensheathed wires each). At the proximal end of the specimen, the 15 wires were attached to distinct contacts on a custom-designed PCB for electrical connections. At the distal end, the wires in each of the secondary bundles were shorted together (after exiting the silicone tubing) and attached to contact pins (Figure 3B).

In this test setup, the TFJ was clamped by a fixture that oscillated in a manner that flexed the TFJ at the exit point for the three secondary bundles (Figure 6). The three secondary bundles were kept in slight tension by attaching a single 3-gram weight about 7 cm distal to the TFJ; the guide prevented side-to-side movement of the secondary bundles but did not restrict vertical movement. At the distal end, the wires in each of the secondary bundles were shorted with conductive epoxy (Chemtronics CW-2460) and used as a common ground. The common ground and the PCB at the proximal end of the specimen were connected to a system that enabled periodic measurements of individual wire resistance to assess continuity. The PCB connector was mounted with sufficient slack in the primary bundle to avoid significant strains on it during this test.

2.3.3. Secondary Bundle Exit Point and Nerve Suture Points Linear Strain Test —Representing a secondary bundle, each specimen used in this test was comprised of five electrode wires coiled and ensheathed in silicone, from which they exited into individual wires. The individual wires had a ~2 mm long exposed region (ER) 2 cm from the point at which they exited the sheath and tungsten needles were welded to the distal end (Figure 3C). Each test specimen was pre-conditioned in saline at body temperature (37 °C ± 5 °C) for 10 to 15 days, based on the ISO-14708 industry standard for active implantable medical devices [44–47]. Prior to installation in the test setup, each electrode wire in the specimen was bent by 180° at the bundle exit point where the individual wire exited the ensheathed bundle to simulate the extremes of bending strain that may occur during the implantation procedure.

The linear strain test setup (Figure 7A) consisted of three small silicone tubes (Nusil, 1.47 mm ID, 1.96 mm OD, wall thickness: ~0.24 mm), fixed next to each other at one end and attached to a piston at the other. The silicone tubes were used to provide a compliant substrate that could undergo longitudinal strain; the three-tube configuration (Figure 7B) was employed in order to simulate placement of LIFEs in multiple fascicles of a large diameter nerve, which would increase the tendency to bend at the bundle exit point. The piston mechanism used a brushless motor with integrated speed controller coupled to a linear motion assembly to apply longitudinal cyclic strain to the tubes. All five electrode wires from an individual test specimen were attached to the tubes by anchoring the coiled ensheathed bundle (CS2–4) to the middle tube with suture at point T1, then suturing the individual wire electrodes in groups of two and three to the outer tubes. These sutures (T3 and T4) simulate the restraining effect of the epineurium on each electrode wire as it enters and exits the nerve. Finally, all five electrode wires were anchored together to the middle tube at suture point T2 before removing the tungsten needles. The specimen was submerged in a bath of saline (0.9% NaCl solution) and a silver/silver chloride (Ag/AgCl) reference electrode was inserted in the bath to allow impedance monitoring and recording.

2.4. Test Paradigms

Given the highly variable nature of activities typically performed with the arm, each test was performed to evaluate fatigue under one of the following test paradigms: a high repetition/low amplitude paradigm to test the effects of arm movement on the leads during activities such as walking (GAIT paradigm). A low repetition/high amplitude paradigm to test the effects of strenuous upper arm activities such as reaching/lifting and/or athletic activities (REACH paradigm). Testing parameters for each paradigm are listed in Table 1. The table indicates the cycle rate (rate at which the strain is being applied), amplitude (level of strain and repetitions), and the number of cycles performed.

2.4.1. Testing Amplitude

ISR Primary Bundle Exit Linear and Angular Strain Amplitudes: The strains experienced by the ISR primary bundle during walking are not expected to be substantial due to the low amplitude of arm movement and low levels of muscle contractions. In addition, deltoid contraction mainly happens during shoulder abduction, which does not normally take place during walking. Furthermore, since there is ample slack in the primary bundle (CS1), it is unlikely that it will experience significant linear or angular strains during tasks such as walking. Consequently, tests using the GAIT paradigm were not performed for the ISR primary bundle exit site.

However, despite the considerable slack in the CS1 portion of the lead, it may be subject to linear and angular strains that would concentrate stress at the primary bundle exit point of the ISR can during activities such as reaching. To investigate the fatigue resistance of the primary bundle in the REACH paradigm, ISR primary bundle exit specimens were subjected to a linear strain magnitude of 10% at three different orientations for this section of the implant.

Industry standards for cochlear implants with implantable cans and RF coils [47], recommend angular strain testing of the lead (primary bundle) exit point at ±15° for at least 100,000 cycles. Given that the ISR can is going to be placed in the arm, the primary bundle exit from the can could be subject to more strain than that of a cochlear implant. However, we do not expect it to be more than ±15° because of the compliance of the tissue relative to the rigidity of the ISR. Using a conservative approach, the ISR primary bundle exit angular strain tests in the REACH paradigm were performed at ±45°.

Trifurcation Junction Angular Strain Amplitudes: Based on industry standards [47], the fatigue resistance of the TFJ to angular strain during walking (GAIT paradigm) was tested by subjecting it to bending at ±15°. For the high amplitude (REACH paradigm), specimens were subjected to bending at ±45°.

Secondary Bundle Exit Point and Nerve Suture Points Linear Strain Amplitudes: Although the lead system is not designed to cross the elbow or shoulder, movement of these joints contributes to the magnitude of the strain that peripheral nerves in the upper arm and, hence, the lead system could experience. During walking, the elbow and shoulder each undergo an excursion that is less than 1/3 that which is expected for maximum nerve strain of around 22% [27]. Kinematic analysis during normal gait indicates that the elbow joint goes through an excursion of approximately 20° [48]. Topp et al. have reported a 22% strain at elbow flexion of 140° [28]. The expected strain during walking was calculated as the product of maximum strain (22%) times the ratio of the angular excursion during gait (20°) and the maximum excursion (140°). This calculation produces an estimate of less than 3.3% strain during the gait cycle; the low amplitude tests (GAIT paradigm) were performed at 5% strain.

To simulate the amount of strain induced by high amplitude activities such as reaching/lifting and/or athletic activities, amplitude values were selected based on postures that maximize strain on the nerves. Neurodynamic mobilization studies in cadavers by Coppieters et al. [29] showed peak strain levels of approximately 6% and 9.8% in the median and ulnar nerves, respectively, at sites about 10 cm proximal to the elbow that are comparable to the sites where the ISR electrode wires are designed to be implanted in the nerves. These measurements were made while performing nerve-tensioning techniques, which put the arm in a posture designed to maximally elongate the nerve bed. For the median nerve, this consisted of simultaneously extending the wrist from 0–60° and extending the elbow from 90–180°. For the ulnar nerve, it consisted of simultaneously extending the wrist by 60°, while fully flexing the elbow, and abducting the shoulder by 100° along with arm supination. Topp et al. report higher strain values of around 22% in some cases during maximum elbow flexion as recorded from cadaver studies, however these recordings were made near the elbow joint, which is expected to experience higher strains than at the implant site [28].

Based on these reported values, it is expected that the implant sites in the median or ulnar nerves, that are proximal to the elbow, would not experience strains over 10% even when flexing muscles in the upper arm while lifting and manipulating objects. A strain level of 15% was selected for use in the high amplitude tests (REACH paradigm).

2.4.2. Testing Repetitions and Rates—The fatigue tests were designed to assess the viability of the electrode lead system for a minimum of 2 years, and therefore the number of repetitions (cycles) for each test was set accordingly. For the GAIT paradigm scenario, it was assumed that an average person will walk about 10,000 steps a day or perform less than 10,000 shoulder/elbow rotations [49]. This translates to >7.3 million repetitions over 2 years.

The REACH scenario was intended to mimic strain that might be applied during highly strenuous reaching/lifting or athletic activity but these are well beyond the strain levels that are anticipated to be induced during most daily activities. Based on guidelines the US Occupational Safety and Health Administration (OSHA) [50], we anticipated that a person might perform moderate activities (lift 25 pounds six times per minute) for 4 hours per day or very heavy activities (lift 25 pounds more than 13 times per minute) for 2 hours per day. These scenarios result in a maximum of 1680 cycles per day or >1.22 million cycles over 2 years.

The ISR primary bundle exit linear and angular strain tests were performed for a total of 1.55 million and 1.33 million cycles respectively, under the REACH paradigm. The trifurcation junction angular strain test was performed for a total of 7.4 million cycles under the GAIT paradigm, and 1.36 million cycles under the REACH paradigm. Finally, the secondary bundle exit point and nerve suture points linear strain test were performed for a total of 7.5 million cycles under the GAIT paradigm, and 1.28 million cycles under the REACH paradigm.

Cycle rates of 2 cycles/sec and 3 cycles/sec were chosen for all angular and linear strain tests, respectively. This was done in order to balance the needs of completing the tests within a reasonable amount of time without introducing any additional failure mechanisms. However, it should be noted that these rates were higher than the physiologically observed value (rate of arm motion during walking < 2 cycles/sec [48, 51]).

2.5. Data collection

2.5.1. Continuity and Impedance Measurements—Lead wire continuity for the ISR lead exit and trifurcation junction test specimens was assessed before and after each test. This assessment was done using a digital multimeter (Meterman HD160B) to directly measure the resistance between the contacts in the PCB DB25 connector and the distal end of the wires, which were shorted to a common ground.

Electrode impedances were recorded using a measurement system that applied a constant current biphasic square pulse (75 μA; 25 μs) and measured the voltage drop during the first phase. A pure silver wire embedded in a small Ag/AgCl pellet (0.8 mm × 3mm) was used as the reference electrode.

Electrode impedances of the secondary bundle exit point and suture points test specimen were obtained before and after installation on the test setup to confirm that pre-test handling did not induce substantial damage. Impedance monitoring during all tests was also performed once per minute to detect if and when an electrode failure occurred. A final impedance measurement was performed after completion of all tests to assess lead integrity.

The impedance values for the electrodes tested during the secondary bundle exit point and suture points linear strain tests should be between 5kΩ – 10kΩ [8, 41, 52, 53]. The impedance failure threshold for detecting wire breakage was selected by recording the impedance values after different types of intentionally caused wire damage. In preliminary tests, the average impedance readings collected for complete wire and insulation breakage in a saline solution was ~34kΩ (as recorded by the impedance measurement system used throughout all tests). For samples with partial damage (wire breakage with intact insulation), an open circuit was detected. Based on these recordings, an impedance threshold value of 17kΩ was selected to detect breakage.

2.5.2. Visual Inspections—Each test specimen was carefully inspected for damage to the wires and the protective silicone sheathing before and after installation on their respective test setup. Pre-test (before and after installation) and post-test photographs of each stress riser point were taken using a Nikon D3200 digital camera mounted on a zoom stereo microscope with 10X magnification.

3. Results

Fatigue testing of each stress riser point was completed using the series of modular mechanical setups described above in order to apply repetitive linear or angular strains to the test specimens. Depending on the testing paradigm used, the specimens were tested for either >1.22 million or >7.3 million cycles. All test setups remained stable with no sign of mechanical breakdown throughout the duration of the study. The mechanisms performed as designed, applying uninterrupted linear or angular strains to the test specimens.

3.1. ISR Lead Exit

3.1.1. Continuity measurements and visual inspection revealed no damage at the ISR lead exit—All test specimens exhibited normal electrical continuity after completion of the linear and angular strain fatigue tests. Table 2 shows the resistance values collected before and after each test, which indicated that the test procedures had no effect on wire resistance. The leads were inspected with a microscope following fatigue testing; strain was applied around the ISR primary bundle exit in each specimen during inspection to reveal any cracks in the silicone. Visual inspection did not reveal any visible cracks in the protective silicone tubing around the electrode leads exiting the ISR. Based on the electrical continuity and visual inspection, no damage was found in any of the wires.

3.2. Trifurcation Junction

3.2.1. Continuity measurements and visual inspection revealed no damage at the TFJ—All test specimens exhibited normal electrical continuity after the TFJ had been subjected to the angular strain fatigue test. Table 3 shows the resistance values collected before and after each test, which indicated that the test procedures had a very small effect on wire resistance (< 2% change). The secondary bundles were inspected with a microscope following fatigue testing; strain was applied around the TFJ of each specimen during inspection to reveal any cracks in the silicone. Visual inspection did not reveal any visible cracks on the protective silicone tubing around the electrode wires in each of the secondary

bundles exiting the TFJ. Based on the electrical continuity and visual inspection, no damage was found in any of the wires.

3.3. Secondary Bundle Exit Point and Nerve Suture Points

3.3.1. Impedance measurements revealed no individual wire damage—All test specimens exhibited impedance values below the failure threshold throughout the fatigue tests. Final impedance values were 4.04±0.44kΩ for the specimens tested in the GAIT paradigm (n=10), and 3.67±0.50kΩ for the specimens tested in the REACH paradigm (n=9). One of the electrodes in one of the samples tested during the REACH paradigm was ignored since its pre-test impedance was more than 20kΩ. This was likely caused by damage to the electrode wire during fabrication, packaging or handling prior to the test. Based on the electrode design specifications, the electrode itself was deemed unusable prior to testing.

3.3.2. Visual inspection did not reveal damage to the bundle exit point or suture points—High magnification photographs of the test specimens following fatigue testing showed that T1 and T2 sutures remained intact and all electrode wires remain sutured at the distal end (T2). No breaks or sharp bends were found on any of the electrode wires. Finally, there were no visible cracks in the coil sheath at the proximal suture point (T1).

4. Discussion

To the best of our knowledge, this is the first report of a study evaluating the fatigue resistance of a LIFE-based branched electrode lead system. Some of the equipment and procedures developed for this study were similar to those used to test other implantable lead systems such as those found in cochlear implants. These tests, however, were designed to expose the ISR lead system to conditions that mimic anticipated strain profiles in the upper arm. While the test parameters described in this paper are specific to our system (ISR device with LIFEs implanted in nerves in the upper arm), these setups and procedures can be implemented to test other peripheral nerve electrode lead systems.

Tests were performed at various stress riser points on representative specimens of the implantable lead system. Representative test specimens were manufactured using identical materials and equivalent manufacturing process as that of the final device for human use. The critical stress riser points that were identified include the ISR lead exit from the can, the trifurcation junction, the point where the individual wires exit the bundle and the nerve suture points. Examination of the test specimens by impedance, electrical continuity measurements, and visual inspection under high magnification microscope did not reveal any noticeable signs of damage due to fatigue at the different stress riser points. Since the levels of strain applied during testing were designed to be higher than those expected at the implant site, these results suggest that the electrode lead system would maintain functionality after deployment in the upper arm. Confirmation of these results will require longitudinal studies *in vivo*.

4.1. Design of Test Setups

Each test setup used in this study was custom-designed and built in-house due to the lack of suitable commercially available equipment. 3D-printed parts as well as some off-the-shelf components were used to assemble different modules in each test setup. The modular design allowed for adjustments on each sub-assembly as testing parameters were fine-tuned.

The TFJ test apparatus was designed to apply angular strain to the three smaller secondary bundles of coiled wires ensheathed in silicone as they exit the trifurcation junction. General guidelines for flexural stress testing listed in established industry standards [46, 47] were followed to define specific testing conditions applicable to our TFJ design. The holding fixture was made of rigid material, with a corner (in contact with the TFJ) rounded to a maximum radius of < 0.5 mm. The branched bundles were attached together to a single 3-gram weight in order to straighten them and simulate slight pulling by muscles and tissue. A guiding rail around the weight prevented pendulum-like swinging of the leads as the angular strain was applied to the junction. The specimen positioning used in this setup guaranteed that the bending occurred exactly at the point of the trifurcation where a drastic change in shape and stiffness could increase stress concentration.

While the secondary bundle exit point, electrode wires, and suture points were tested while exposed to saline solution during the linear strain test, the trifurcation junction was not. The silicone material used in the protective sheathing and trifurcation junction is the same as that used in cochlear implants. Furthermore, the safety and reliability of all the materials used in our implantable lead system in a physiological environment is well documented [8, 41, 42, 54] and no further testing in a saline environment was deemed necessary.

The secondary bundle exit point and suture points linear strain test apparatus was designed using a test specimen holder with a three-tube configuration. This was done in order to spread out the wires in a manner that is similar to what is expected during human implantation. The nerve is slightly larger than the branched bundles and the orientation of the secondary bundle exit point might be different from the electrode nerve entry points. Therefore, the electrode wires are expected to fan out. For this test, the electrode wires were installed employing procedures similar to those that will be used during surgery. However, instead of inserting the electrode wires, inside the tube as would be done for nerves during the surgical procedure, they were sutured to the outer surface of the tubes. The silicone tubing wall is stiffer than what is expected in the nerve tissue [55]. Traversing the tube wall could therefore have induced damage to the electrode wires that would not be representative of conditions expected in the nerve. Instead, sutures were used to hold the electrode wires in place at the points where they would have entered and exited the nerve.

4.2. Selection of test parameters

4.2.1. ISR primary bundle exit: linear and angular strain amplitude considerations—In human implants, the ISR can will be placed on the lateral side of the upper arm. The can will be anchored at the point where the deltoid inserts into the humerus. This anchoring location was selected to provide good stability in a location that is near the surface of the skin. The single primary electrode bundle (CS1) exiting the ISR can will be

implanted to follow a path that goes distally from the can and then traverses the arm anterior to the humerus and posterior to the brachialis and biceps. On the medial side, the bundle will have slack, with the three prongs of the trifurcation junction pointing distally and the branched secondary electrode bundles aligned parallel to the nerves. The primary and branched secondary bundles with ensheathed coiled wires are flexible and will have adequate slack to avoid concentration of stress at any single point along their length. Nonetheless, our test design did not account for such slack in order to test for a worst-case scenario. There are no established testing standards for this particular design and deployment of the lead. Consequently, the selected values for strain amplitudes were chosen based on established industry standards for comparable implantable medical devices [47]. The conservative safety factors used to account for differences in anatomical locations may have greatly exceeded what will be experienced *in vivo*.

4.2.2. Trifurcation junction test amplitude considerations—The TFJ angular strain test for the low amplitude (GAIT) condition was performed at ±15°. However, it is unlikely that the secondary bundle branches that exit the trifurcation junction will experience significant angular strain during low amplitude tasks such as walking. The angular strain amplitude applied during the high amplitude (REACH) condition was ±45°, which was intended to simulate high amplitude physical activities, and is more than what is expected at the implant location.

4.2.3. Secondary bundle exit point and nerve suture points linear strain test amplitude considerations—In the intended application of this system, the electrode wires will be implanted in the median and ulnar nerves approximately 10 cm above the medial epicondyle in the upper arm, which is a region that is expected to see much less strain than the sites closer to the elbow joint. The nerve tensioning technique used by Coppieters et al. was meant to stretch the nerves as much as possible and a strain of 9.8% reported was at a site proximal to the elbow joint, which is approximately where the electrode wires will be implanted in the nerves. Studies in rodents have shown that nerve strain occurs most prominently in the highly compliant nerve segments at the elbow and shoulder joints, while nerve segments distant from the joints experience progressively lower levels of strain [26]. Cadaver studies reported by Topp et al. include movements of the wrist joint. Median nerve studies have shown that wrist movements have some effect on strain levels [29]. Since the ISR is going to be implanted in transradial amputees who do not have a wrist, they would not be subject to that component of strain.

4.2.4. Testing repetitions and rates—In this study, we tested specimens for over 1 million cycles in the high-amplitude paradigm and for over 7 million cycles in the low-amplitude test paradigm. These numbers were derived for aggressive activity levels sustained over a period of 2 years and were significantly higher than what is expected for active implantable devices. Industry standards for comparable active implantable medical devices [47] recommend testing electrode lead systems for at least 100,000 cycles. These are particular requirements for cochlear devices and do not meet the specific needs for conditions relevant to peripheral nerve interfaces as described here. Our test parameters far exceed these industry standards and no failures were observed.

Cycle rates of 2 cycles/sec and 3 cycles/sec were chosen for all angular and linear strain tests, respectively. These test rates allowed us to expose the specimens to velocity and acceleration levels that are higher than physiologically observed values. Some physical activities involving high velocity elbow excursion could induce high velocity nerve stretch at the implant site, affecting the secondary bundle exit point and nerve suture points. For instance, a professional baseball pitcher experiences maximum elbow excursion angular velocity just before the ball is released. At this point, the mean angular velocity may reach up to 2,500 degrees per second [56–58]. These velocities are seen mostly in professional athletes and are unlikely to be experienced by amputees. The parameters used for testing these components under linear strains exposed the specimens to peak angular velocities of about 30,000°/sec during the GAIT condition, and about 90,000°/sec during the REACH condition. Finally, the ISR primary bundle exit and trifurcation junction will not be tethered to the nerve, therefore they are unlikely to be directly affected by high velocity nerve stretch. These lead system components were tested for peak angular velocities of 550–600°/sec.

4.3. Test measurements

The electrical and visual verification protocols used in this study may not have been sensitive enough to determine whether micro-cracks were present in the electrode wire insulation. This type of damage could weaken the electrode wires in a manner that would eventually result in failure. However, the presence of micro-cracks would not significantly affect the electrical performance of the electrodes. The micro-cracks would have a high impedance relative to the active area, preventing the charge from leaking through the cracks. Moreover, the protective silicone tubing used for ensheathing the wire bundles is backfilled with silicone, which prevents wire movement and reduces the risk of damage and acts as a barrier between the conducting material and the surrounding biological environment in case of insulation failure. More extensive studies could include electron microscopy to investigate the presence of microscopic damage.

4.4. Implications for other electrode lead systems

The performance of early cardiac pacing lead systems was traditionally characterized based on hundreds of patient follow-ups over many years [39]. These studies collected information in terms of electrical performance, number of complications and overall longevity. Other early implantable lead systems such as those used for functional electrical stimulation were also tested using *in vivo* animal models to evaluate the mechanical and electrical performance of the leads in growing and moving limbs, before implanting them in human patients [35]. More recent studies have combined *in vivo* animal models, computational models and mechanical fixtures to expose spinal cord stimulation lead systems to repetitive stresses and investigate lead breakage and migration [22]. The results of this study may have an impact on the design of implantable lead systems. Considering the limitations discussed, the equipment and procedures described in this study represent an important step in the evaluation of the mechanical performance of a lead system. The modular and customizable design of the test setups used during this study allows for a variety of configurations that could be used to test components (e.g. coil sheaths, lead exits, bi/trifurcations, and other common stress points) of neural interface systems, including their lead systems. These methods can be used to expose specimens to linear and angular strains, under an appropriate

set of testing parameters and using suitable structures for specimen positioning. Furthermore, the testing intensity could be increased by implementing accelerated fatigue testing techniques such as increased loading rates and/or temperature. Assessment of the performance of the electrode interface itself will be dependent on the type of electrode utilized (e.g. the FINE, Utah electrode array, TIME [4, 9–13]) and depend on the implantation procedures. For LIFEs, long-term viability had previously been demonstrated with electrodes chronically implanted in the radial nerves of cats [8]; the setup and results presented here for the individual wires (Section 2.3.3, Section 3.3) provide additional data to characterize the long term performance of these electrodes in conditions designed to mimic those anticipated in humans. To characterize other electrode types, test setups and protocols would have to be devised to reflect the conditions anticipated for each electrode design.

5. Conclusions

We have evaluated the fatigue resistance of an implantable branched intra-fascicular electrode lead system under conditions similar to or worse than those expected when implanted in the peripheral nerves of upper limb amputees. The test setups and procedures used in this study exposed the electrode lead system to strain profiles that are more intense than those expected in the upper arm. The results presented here suggest that this set of leads and fine-wire electrodes would maintain functionality after deployment in the upper arm of transradial amputees. Furthermore, the test setups and procedures used here may be appropriate for use in the evaluation of other lead systems for peripheral nerve interfaces.

Acknowledgments

The authors would like to thank Anil Thota for his valuable insight for the installation and testing procedures. This work was funded by the National Institutes of Health (NIH) through a National Institute of Biomedical Imaging and Bioengineering (NIBIB) and a National Institute of Child Health and Human Development (NICHD) grant NIH-R01-EB008578

References

1. Romero-Ortega Y-T, Ka MI. Material considerations for peripheral nerve interface. MRS BULLETIN. 2012; 37
2. Grill WM, Norman SE, Bellamkonda RV. Implanted neural interfaces: Biochallenges and engineered solutions. Annu Rev Biomed Eng. 2009; 11:1–24. [PubMed: 19400710]
3. Schachter SC, Saper CB. Vagus nerve stimulation. Epilepsia. 1998; 39:677–86. [PubMed: 9670894]
4. Del Valle J, Navarro X. Interfaces with the peripheral nerve for the control of neuroprostheses. Int Rev Neurobiol. 2013; 109:63–83. [PubMed: 24093606]
5. Dhillon GS, Lawrence SM, Hutchinson DT, Horch KW. Residual function in peripheral nerve stumps of amputees: Implications for neural control of artificial limbs. The Journal of hand surgery. 2004; 29:605–15. [PubMed: 15249083]
6. Kovacs GT, Storment CW, Rosen JM. Regeneration microelectrode array for peripheral nerve recording and stimulation. IEEE Trans Biomed Eng. 1992; 39:893–902. [PubMed: 1473818]
7. Ledbetter NM, Ethier C, Oby ER, Hiatt SD, Wilder AM, Ko JH, Agnew SP, Miller LE, Clark GA. Intrafascicular stimulation of monkey arm nerves evokes coordinated grasp and sensory responses. Journal of Neurophysiology. 2013; 109:580–90. [PubMed: 23076108]
8. Lefurge T, Goodall E, Horch K, Stensaas L, Schoenberg A. Chronically implanted intrafascicular recording electrodes. Annals of biomedical engineering. 1991; 19:197–207. [PubMed: 2048777]

9. Oddo CM, Raspopovic S, Artoni F, Mazzoni A, Spigler G, Petrini F, Giambattistelli F, Vecchio F, Miraglia F, Zollo L, Di Pino G, Camboni D, Carrozza MC, Guglielmelli E, Rossini PM, Faraguna U, Micera S. Intraneural stimulation elicits discrimination of textural features by artificial fingertip in intact and amputee humans. Elife. 2016; 5
10. Schiefer M, Tan D, Sidek SM, Tyler DJ. Sensory feedback by peripheral nerve stimulation improves task performance in individuals with upper limb loss using a myoelectric prosthesis. J Neural Eng. 2016; 13:016001. [PubMed: 26643802]
11. Tyler DJ, Durand DM. Functionally selective peripheral nerve stimulation with a flat interface nerve electrode. Neural Systems and Rehabilitation Engineering, IEEE Transactions on. 2002; 10:294–303.
12. Kundu A, Harreby KR, Yoshida K, Boretius T, Stieglitz T, Jensen W. Stimulation selectivity of the "thin-film longitudinal intrafascicular electrode" (tflife) and the "transverse intrafascicular multi-channel electrode" (time) in the large nerve animal model. IEEE Trans Neural Syst Rehabil Eng. 2014; 22:400–10. [PubMed: 23799699]
13. Davis TS, Wark HA, Hutchinson DT, Warren DJ, O'neill K, Scheinblum T, Clark GA, Normann RA, Greger B. Restoring motor control and sensory feedback in people with upper extremity amputations using arrays of 96 microelectrodes implanted in the median and ulnar nerves. J Neural Eng. 2016; 13:036001. [PubMed: 27001946]
14. Dadd, F., Schuller, P., Pawsey, NCK., Manouchehri, S. Strain relief in an implantable electrode assembly. patent US. 0196465 A1. Aug 11. 2011 inventors. Patent, assignee
15. Greenberg, RJ., Mann, AE., Little, JS., Ihrig, KH., Mech, BV., Talbot, NH., Zhou, DM. Implantable retinal electrode array configuration for minimal retinal damage and method of reducing retinal stress. 2011. inventors. Google Patents, assignee
16. Marsolais EB, Kobetic R. Implantation techniques and experience with percutaneous intramuscular electrodes in the lower extremities. J Rehabil Res Dev. 1986; 23:1–8.
17. Shiroff, JA., Skubitz, JJ., Rawat, PB. Electrode leads for use with implantable neuromuscular electrical stimulator. USA patent. WO2016020846 A1. 2015 Aug 5. inventors. Mainstay Medical Limited, assignee
18. Thota, AK., Jung, R., Kuntaegowdanahalli, SS. Multi-lead multi-electrode management system. USA patent. US9409009 B2. 2013 Nov 6. inventors. The Florida International University, assignee
19. Macdiarmid SA, Peters KM, Shobeiri SA, Wooldridge LS, Rovner ES, Leong FC, Siegel SW, Tate SB, Feagins BA. Long-term durability of percutaneous tibial nerve stimulation for the treatment of overactive bladder. J Urol. 2010; 183:234–40. [PubMed: 19913821]
20. Peters KM, Carrico DJ, Perez-Marrero RA, Khan AU, Wooldridge LS, Davis GL, Macdiarmid SA. Randomized trial of percutaneous tibial nerve stimulation versus sham efficacy in the treatment of overactive bladder syndrome: Results from the sumit trial. J Urol. 2010; 183:1438–43. [PubMed: 20171677]
21. Laing, B., Green, JD. Percutaneous tibial nerve stimulator. USA patent. US8660646 B2. 2012 Jun 15. inventors. Advanced Uro-Solutions, Llc, assignee
22. Henderson JM, Schade CM, Sasaki J, Caraway DL, Oakley JC. Prevention of mechanical failures in implanted spinal cord stimulation systems. Neuromodulation. 2006; 9:183–91. [PubMed: 22151706]
23. Machado A, Rezai AR, Kopell BH, Gross RE, Sharan AD, Benabid AL. Deep brain stimulation for parkinson's disease: Surgical technique and perioperative management. Mov Disord. 2006; 21(Suppl 14):S247–58. [PubMed: 16810722]
24. Weber DJ, Friesen R, Miller LE. Interfacing the somatosensory system to restore touch and proprioception: Essential considerations. Journal of motor behavior. 2012; 44:403–18. [PubMed: 23237464]
25. Saal HP, Bensmaia SJ. Biomimetic approaches to bionic touch through a peripheral nerve interface. Neuropsychologia. 2015
26. Phillips JB, Smit X, De Zoysa N, Afoke A, Brown RA. Peripheral nerves in the rat exhibit localized heterogeneity of tensile properties during limb movement. J Physiol. 2004; 557:879–87. [PubMed: 15064329]

27. Tillett RL, Afoke A, Hall SM, Brown RA, Phillips JB. Investigating mechanical behaviour at a core-sheath interface in peripheral nerve. J Peripher Nerv Syst. 2004; 9:255–62. [PubMed: 15574138]
28. Topp KS, Boyd BS. Structure and biomechanics of peripheral nerves: Nerve responses to physical stresses and implications for physical therapist practice. Phys Ther. 2006; 86:92–109. [PubMed: 16386065]
29. Coppieters MW, Butler DS. Do 'sliders' slide and 'tensioners' tension? An analysis of neurodynamic techniques and considerations regarding their application. Man Ther. 2008; 13:213–21. [PubMed: 17398140]
30. Keith MW, Peckham PH, Thrope GB, Buckett JR, Stroh KC, Menger V. Functional neuromuscular stimulation neuroprostheses for the tetraplegic hand. Clin Orthop Relat Res. 1988:25–33.
31. Keith MW, Peckham PH, Thrope GB, Stroh KC, Smith B, Buckett JR, Kilgore KL, Jatich JW. Implantable functional neuromuscular stimulation in the tetraplegic hand. J Hand Surg Am. 1989; 14:524–30. [PubMed: 2786897]
32. Kilgore KL, Peckham PH, Keith MW, Thrope GB. Electrode characterization for functional application to upper extremity fns. IEEE Trans Biomed Eng. 1990; 37:12–21. [PubMed: 2154398]
33. Memberg WDP, Thrope PH, Keith GB, Kicher MW, TP. An analysis of the reliability of percutaneous intramuscular electrodes in upper extremity fns applications. Rehabilitation Engineering, IEEE Transactions on. 1993; 1:7.
34. Smith BT, Betz RR, Mulcahey MJ, Triolo RJ. Reliability of percutaneous intramuscular electrodes for upper extremity functional neuromuscular stimulation in adolescents with c5 tetraplegia. Arch Phys Med Rehabil. 1994; 75:939–45. [PubMed: 8085926]
35. Akers JM, Smith BT, Betz RR. Implantable electrode lead in a growing limb. IEEE Trans Rehabil Eng. 1999; 7:35–45. [PubMed: 10188606]
36. Kilgore KL, Peckham PH, Keith MW, Montague FW, Hart RL, Gazdik MM, Bryden AM, Snyder SA, Stage TG. Durability of implanted electrodes and leads in an upper-limb neuroprosthesis. J Rehabil Res Dev. 2003; 40:457–68. [PubMed: 15077658]
37. Levander-Lindgren M. A 20-year study of endocardial pacing lead emt 588. Lead durability and nature of failure. Scand J Thorac Cardiovasc Surg. 1988; 22:1–6. [PubMed: 3387942]
38. Helguera ME, Maloney JD, Woscoboinik JR, Trohman RG, Mccarthy PM, Morant VA, Wilkoff BL, Castle LW, Pinski SL. Long-term performance of epimyocardial pacing leads in adults: Comparison with endocardial leads. Pacing Clin Electrophysiol. 1993; 16:412–7. [PubMed: 7681192]
39. Kazama S, Nishiyama K, Machii M, Tanaka K, Amano T, Nomura T, Ohuchi M, Kasahara S, Nie M, Ishihara A. Long-term follow up of ventricular endocardial pacing leads. Complications, electrical performance, and longevity of 561 right ventricular leads. Jpn Heart J. 1993; 34:193–200. [PubMed: 8315816]
40. Thota AK, Kuntaegowdanahalli S, Starosciak AK, Abbas JJ, Orbay J, Horch KW, Jung R. A system and method to interface with multiple groups of axons in several fascicles of peripheral nerves. J Neurosci Methods. 2015; 244:78–84. [PubMed: 25092497]
41. Dhillon GS, Horch KW. Direct neural sensory feedback and control of a prosthetic arm. Neural Systems and Rehabilitation Engineering, IEEE Transactions on. 2005; 13:468–72.
42. Patrick JF, Busby PA, Gibson PJ. The development of the nucleus freedom cochlear implant system. Trends Amplif. 2006; 10:175–200. [PubMed: 17172547]
43. Pilkey, WD., Pilkey, DF. Peterson's stress concentration factors. 3. Hoboken, NJ: John Wiley; 2008. p. 522
44. International Standards Office. ISO 14708 implants for surgery - active implantable medical devices, part 1: General requirements for safety, marking and for information to be provided by the manufacturer. Geneva: ISO; 2014.
45. International Standards Office. ISO 14708 implants for surgery - active implantable medical devices, part 3: Implantable neurostimulators. Geneva: ISO; 2017.
46. International Standards Office. ISO 14708 implants for surgery - active implantable medical devices, part 6: Particular requirements for active implantable medical devices intended to treat tachyarrhythmia (including implantable defibrillators). Geneva: ISO; 2010.

47. International Standards Office. ISO 14708 implants for surgery - active implantable medical devices, part 7: Particular requirements for cochlear implant systems. Geneva: ISO; 2013.
48. Collins SH, Adamczyk PG, Kuo AD. Dynamic arm swinging in human walking. Proceedings of the Royal Society B: Biological Sciences. 2009; 276:3679–88. [PubMed: 19640879]
49. Bohannon RW. Number of pedometer-assessed steps taken per day by adults: A descriptive meta-analysis. Phys Ther. 2007; 87:1642–50. [PubMed: 17911274]
50. Occupational Safety and Health Administration. Estimating work rates or loads [Internet]. Occupational Safety and Health Administration; 2011. [cited 2016 Nov 11]. Available from: https://www.osha.gov/SLTC/heatillness/heat_index/work_rates_loads.html
51. Pachi A, Ji T. Frequency and velocity of people walking. The Institution of Structural Engineers. 2005; 83:36–40.
52. Malagodi MS, Horch KW, Schoenberg AA. An intrafascicular electrode for recording of action potentials in peripheral nerves. Ann Biomed Eng. 1989; 17:397–410. [PubMed: 2774314]
53. Lawrence SM, Dhillon GS, Horch KW. Fabrication and characteristics of an implantable, polymer-based, intrafascicular electrode. J Neurosci Methods. 2003; 131:9–26. [PubMed: 14659819]
54. Thota, ASK., Horch, K., Abbas, J., Jung, R. Biocompatibility testing of an implantable intrafascicular electrode system in rabbits. Program No. 522.12. 2015 Neuroscience Meeting Planner; Chicago, Illinois: Society for Neuroscience; 2015. Online
55. Sunderland S, Bradley K. Stress-strain phenomena in denervated peripheral nerve trunks. Brain. 1961; 84:125–7.
56. Feltner M, Dapena J. Dynamics of the shoulder and elbow joints of the throwing arm during a baseball pitch. International Journal of Sport Biomechanics. 1986; 2:235–59.
57. Matsuo T, Escamilla RF, Fleisig GS, Barrentine SW, Andrews JR. Comparison of kinematic and temporal parameters between different pitch velocity groups. J Appl Biomech. 2001; 17:1–13.
58. Werner SL, Fleisig GS, Dillman CJ, Andrews JR. Biomechanics of the elbow during baseball pitching. J Orthop Sports Phys Ther. 1993; 17:274–8. [PubMed: 8343786]

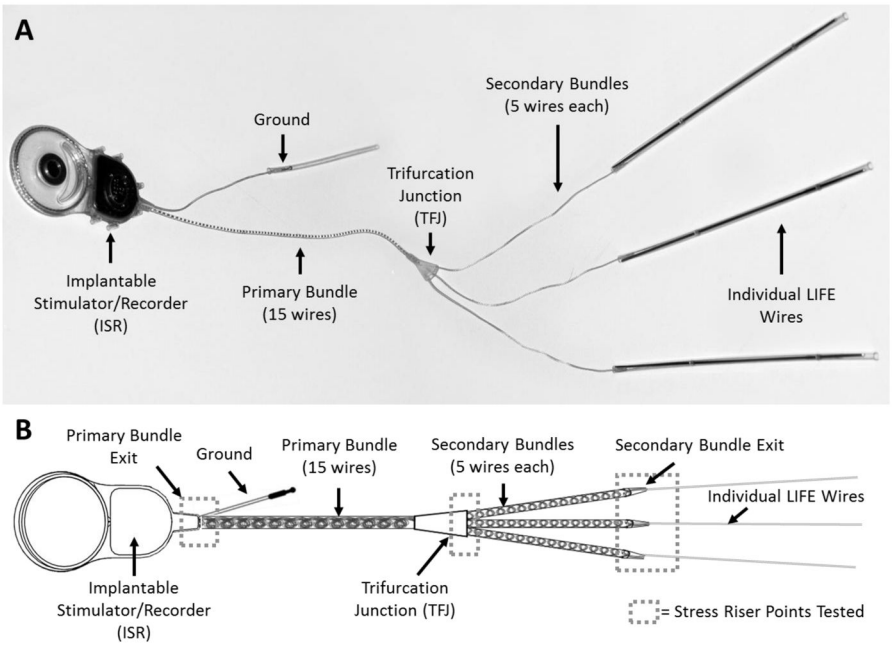

Figure 1.

Implantable components of the stimulator/recorder with a branched lead system and longitudinal intrafascicular electrodes (LIFEs). A) Picture of the implantable neural stimulator/recorder. B) Schematic of the implantable neural stimulator/recorder showing the stress points that were tested (dashed boxes). The device is comprised of an implantable stimulator/recorder (ISR) unit with a 15-wire lead assembly that consists of a primary silicone ensheathed bundle that leads to a trifurcation junction (TFJ) to form 3 secondary silicone ensheathed bundles, each of which further separates into individual wires (LIFEs). Each LIFE is a 23μm diameter insulated Pt/Ir wire with a 1mm long active zone. When implanted, the ISR primary bundle exit, the TFJ, and the secondary bundle exit are considered to be stress riser points (dashed boxes).

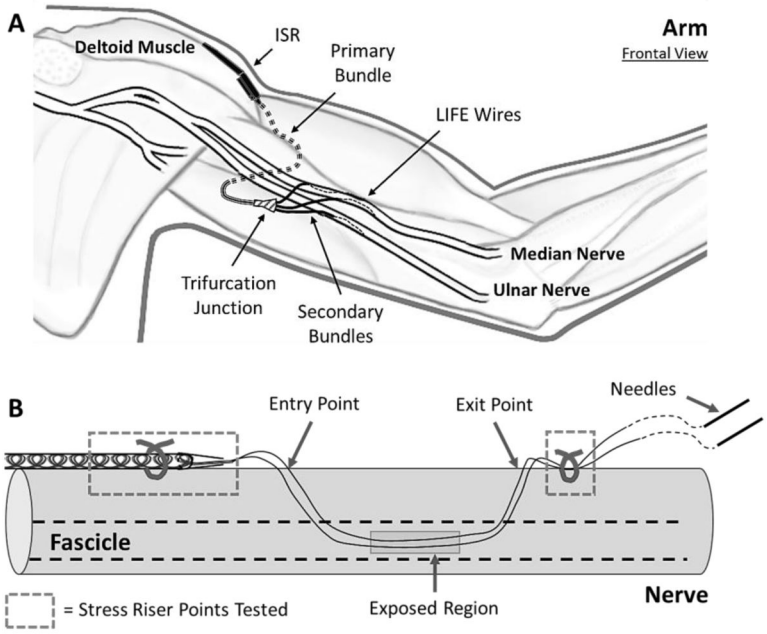

Figure 2.

A) Schematic showing the positioning of the implanted electrode lead system within the upper arm. The ISR can is placed on the lateral side of the upper arm, anchored at the point where the deltoid inserts into the humerus. The primary bundle traverses the arm anterior to the humerus and posterior to the brachialis and biceps. The three prongs of the trifurcation junction point distally and the branched secondary electrode bundles are aligned parallel to the nerves. The individual LIFE wires are implanted longitudinally into a nerve fascicle. B) Schematic showing electrode wires implanted in a nerve fascicle (indicated by dashed lines). During the implantation procedure, each electrode wire is threaded into the nerve fascicle using a tungsten needle attached at the distal end of the wire. Once all the electrode wires from a given coiled ensheathed bundle are implanted, the longitudinal position of the active area is adjusted so that it is within the fascicle. Subsequently, the distal ends of the wires are cut to remove the tungsten needles. The bundle exit point and the remaining portion of the distal wires left outside the nerve are sutured to the epineurium. When implanted, the point where the individual wires exit the silicone sheath (bundle exit) and the nerve suture points are considered stress riser points (dashed boxes).

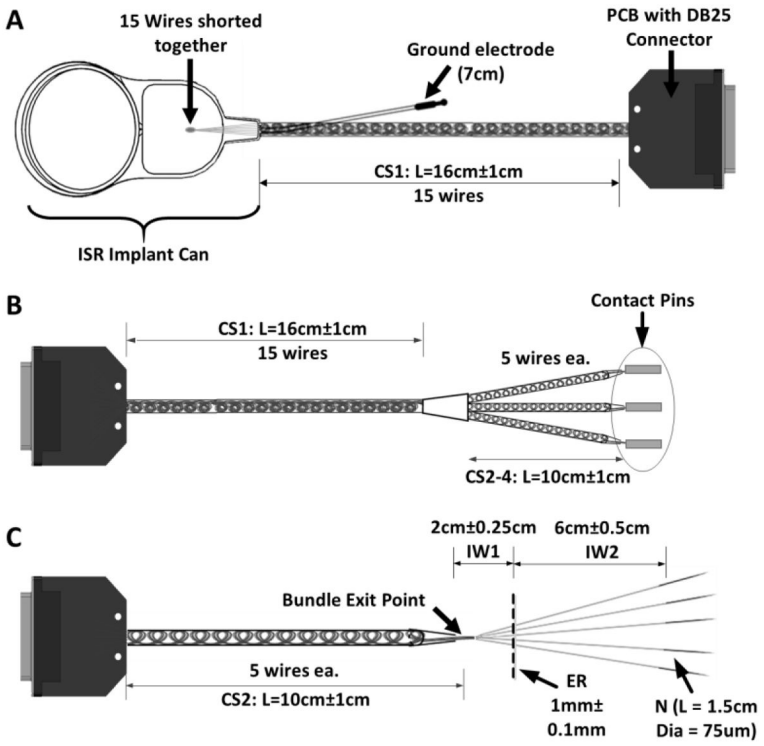

Figure 3.

Schematics of the test specimens used for the evaluation of the stress riser points. A) The ISR bundle exit test specimen used in both linear and angular strain tests consisted of an ISR can, a single primary bundle with 15 coiled ensheathed wires (CS1, L = 15cm), and the ground electrode lead. The distal end of the specimen was connected to distinct contacts on a custom printed circuit connector board (PCB). B) The trifurcation junction angular strain test specimen included a primary bundle with 15 coiled ensheathed wires that trifurcated to form three secondary bundles of five coiled ensheathed wires each (CS2-4). C) The bundle exit and suture points linear strain test specimen included 5 LIFEs (individual wires, IW) exiting a secondary bundle of 5 ensheathed coiled wires (CS2), with the exposed region (ER) 2cm from the bundle exit point and the tungsten needles welded to the distal end.

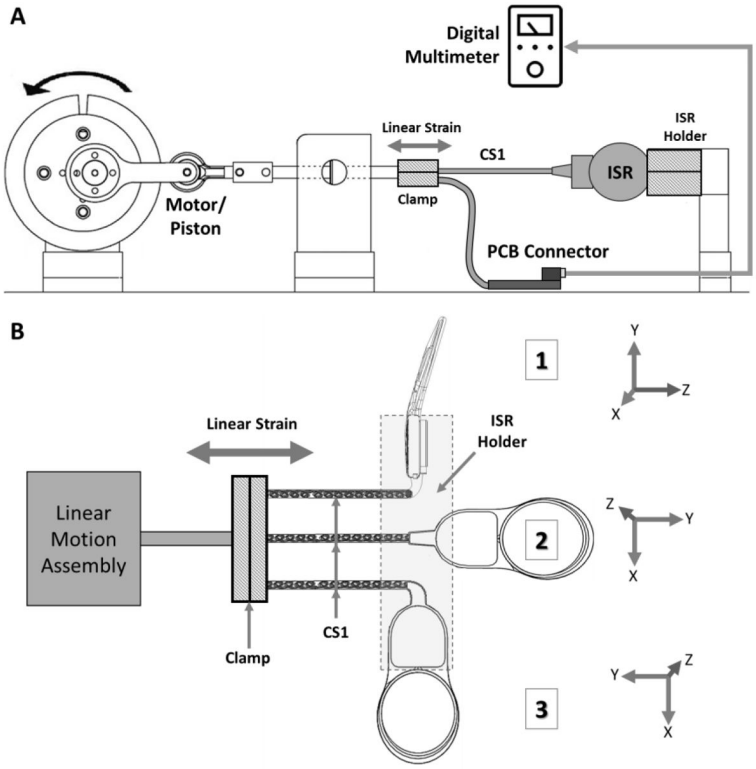

Figure 4.

Schematic of the ISR bundle exit linear strain test setup. A) The setup consisted of a clamping assembly holding three ISR cans in a particular orientation while a portion of the distal end of each bundle with coiled ensheathed wires (CS1) was attached to a piston mechanism. The piston mechanism applied longitudinal cyclic strain to the bundle. Resistance of each of the individual wires in the bundle was monitored using a custom connector board connected to a digital multimeter. B) The three different ISR orientations at which the linear strain was applied 1) 90° bend about the Z and Y-axis; 2) No bend; and 3) 90° bend around the Z-axis. The ISR holder (dashed box) kept the ISR can in place while the distal end of the specimen was clamped to a linear strain system.

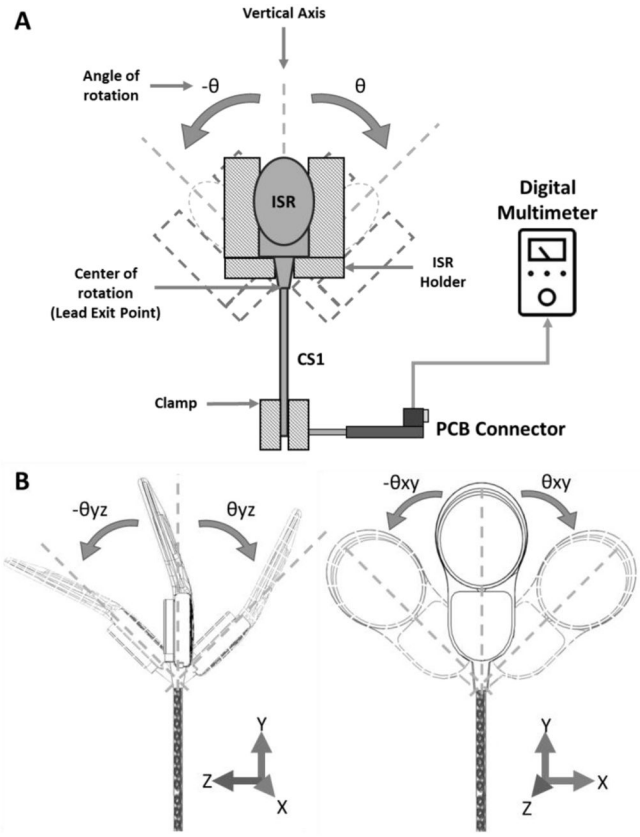

Figure 5.

Schematic of the ISR lead exit angular strain test setup. A) The setup consisted of a swinging fixture designed to hold the ISR at different orientations in order to produce the desired angle of deflection. The fixture was coupled to an oscillating machine that bent the ISR lead at the exit point. The ISR electrode lead exit point was placed at the center of rotation of the mechanism and the distal end of the lead was fixed with a clamp. B) Two different ISR orientations (0° and 90° about the Y-axis) at which the angular strain was applied as the distal end of the specimen was clamped.

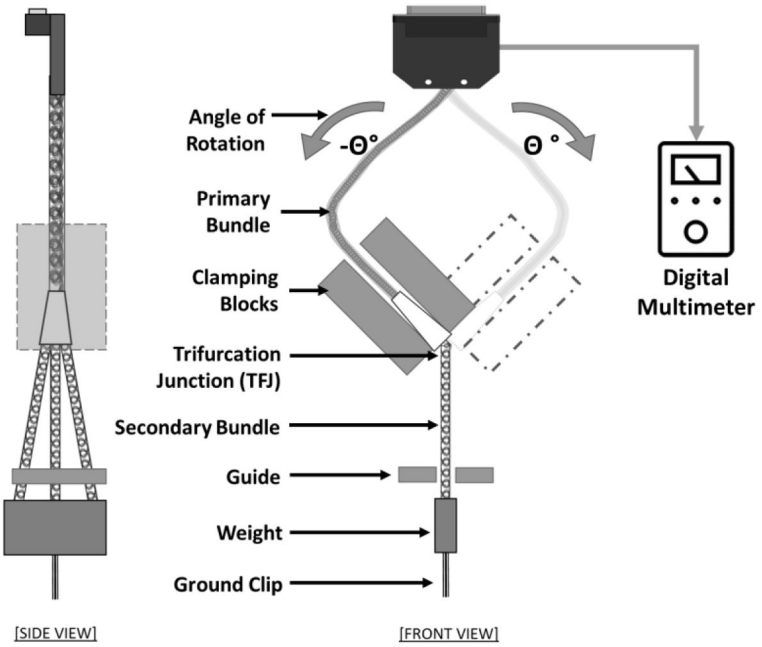

Figure 6.

Schematic of the trifurcation junction angular strain test setup. The TFJ was clamped to a rigid fixture with the three-secondary bundle exit points at the bottom edge. Each of the secondary bundles was passed through a guiding rail (non-contacting at rest position) and kept in slight tension by attaching an appropriate weight (about 3 grams) at the distal end of the three coil sheath tubes to keep the bundle straight. The holding fixture was coupled to an oscillating mechanism that flexed the TFJ at a rate of 2 Hz.

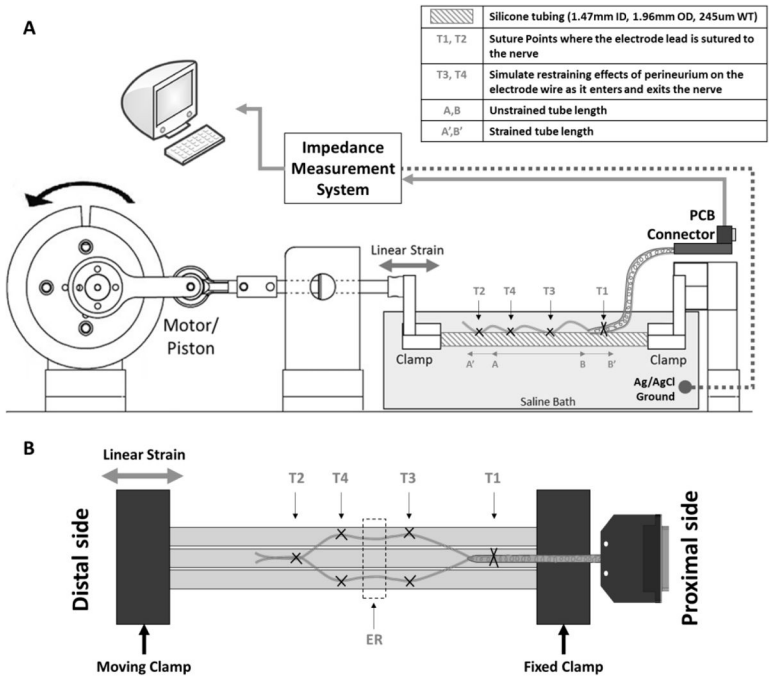

Figure 7.

Schematic of the secondary bundle exit point and nerve suture points linear strain test setup. A) The setup consisted of three small silicone tubes clamped together at one end (fixed clamp) and attached to a piston (moving clamp) at the other. The piston mechanism used a brushless motor coupled to a linear motion assembly to apply longitudinal cyclic strain to the tubes. B) A 3-tube configuration was employed in order to simulate implantation in multiple fascicles of a large diameter nerve. In this configuration, all five electrodes from an individual test specimen were attached to the tubes by anchoring the coil sheath to the middle tube with suture at point T1, then suturing (T3 and T4) the electrodes in groups of two and three to the outer tubes, with the exposed regions (ER) in between. These sutures simulate the restraining effect of the epineurium on each electrode wire as it entered and exited the nerve. Finally, all five electrode wires were anchored to the middle tube at suture point T2, and the tungsten needles were removed.

Table 1

Testing parameters for each test paradigm.

		Test Paradigm			
		GAIT		REACH	
Strain Test performed	**Cycle rate**	**Amplitude**	**Repetitions**	**Amplitude**	**Repetitions**
ISR Lead Exit Linear	3 Cycles/sec	N/A	N/A	10%	1.55M
ISR Lead Exit Angular	2 Cycles/sec	N/A	N/A	±45°	1.33M
Trifurcation Junction Angular	2 Cycles/sec	±15°	7.4M	±45°	1.36M
Bundle Exit And Nerve Suture Points Linear	3 Cycles/sec	5%	7.5M	15%	1.28M

Cycle rate is the rate at which the strain was applied, Amplitude is the level of strain and Repetitions is the number of cycles performed.

Table 2

Resistance recordings from the ISR lead exit tests.

Strain Type	Test Specimen #	Pre-Test Resistance avg ± std (Ω)	Post-Test Resistance avg ± std (Ω)	Average Change %
Linear	1	201 ± 0.83	201 ± 0.83	0
	2	201 ± 0.13	201 ± 0.13	0
	3	201 ± 0.13	201 ± 0.13	0
Angular	4	200 ± 0.13	200 ± 0.13	0
	5	203 ± 0.13	203 ± 0.13	0

Table 3

Resistance recordings from the trifurcation junction angular test.

Test Paradigm	Test Specimen #	Pre-Test Resistance avg ± std (Ω)	Post-Test Resistance avg ± std (Ω)	Average Change %
GAIT	1	262.3 ± 4.9	258.1 ± 1.2	1.57
	2	258.7 ± 0.7	257.8 ± 0.4	0.36
	3	259.6 ± 0.6	258.6 ± 0.4	0.39
REACH	4	262.7 ± 0.9	262.6 ± 0.8	0.05
	5	263.9 ± 4.7	264.0 ± 4.6	0.02